THE JOURNAL OF PHYSICAL CHEMISTRY A

 VOLUME 109, NUMBER 15, APRIL 21, 2005

ARTICLES

NMR Paramagnetic Relaxation of the Spin 2 Complex $Mn^{III}TSPP$: A Unique Mechanism

Nathaniel Schaefle and Robert Sharp*

Department of Chemistry, The University of Michigan, Ann Arbor, Michigan 48109-1055

Received: August 20, 2004; In Final Form: January 26, 2005

The $S = 2$ complex, manganese(III) meso-tetra(4-sulfonatophenyl)porphine chloride ($Mn^{III}TSPP$) is a highly efficient relaxation agent with respect to water protons and has been studied extensively as a possible MRI contrast agent. The NMR relaxation mechanism has several unique aspects, key among which is the unusual role of zero-field splitting (zfs) interactions and the effect of these interactions on the electron spin dynamics. The principal determinant of the shape of the R_1 magnetic relaxation dispersion (MRD) profile is the tetragonal 4th-order zfs tensor component, B_4^4, which splits the levels of the $m_S = \pm 2$ non-Kramers doublet. When the splitting due to B_4^4 exceeds the Zeeman splitting, the matrix elements of $\langle S_z \rangle$ are driven into coherent oscillation, with the result that the NMR paramagnetic relaxation enhancement is suppressed. To confirm the fundamental aspects of this mechanism, proton R_1 MRD data have been collected on polyacrylamide gel samples in which $Mn^{III}TSPP$ is reorientationally immobilized. Solute immobilization suppresses time-dependence in the electron spin Hamiltonian that is caused by Brownian motion, simplifying the theoretical analysis. Simultaneous fits of both gel and solution data were achieved using a single set of parameters, all of which were known or tightly constrained from prior experiments except the 4th-order zfs parameter, B_4^4, and the electron spin relaxation times, which were found to differ in the $m_S = \pm 1$ and $m_S = \pm 2$ doublet manifolds. In liquid samples, but not in the gels, the B_4^4-induced splitting of the $m_S = \pm 2$ non-Kramers doublet is partially collapsed due to Brownian motion. This phenomenon affects the magnitudes of both B_4^4 and electron spin relaxation times in the liquid samples.

Introduction

The $S = 2$ complex, manganese(III) meso-tetra(4-sulfonatophenyl)porphine chloride ($Mn^{III}TSPP$, Figure 1), is a highly efficient relaxation agent with respect to water protons and has been studied extensively as a potential MRI contrast agent.[1−8] At field strengths above 0.25 T, the paramagnetic relation rate, R_{1M}, of water protons bound to the Mn(III) ion is higher[1] than for bound protons in $Mn(H_2O)_6^{2+}$. $Mn^{III}TSPP$ and related Mn(III) porphyrins are the only $S = 2$ spin systems that have been investigated with respect to their NMR−PRE (PRE = paramagnetic relaxation enhancement) properties, and the high inner sphere relaxivity of these complexes was unexpected.[9] Koenig, Brown, and Spillar[1] (KBS) reported magnetic relaxation dispersion (MRD) profiles of the water proton R_1 at three temperatures (shown in Figure 2). They, as well as subsequent studies,[3,8] pointed out that the MRD profiles are unique, both in the magnitude of the proton R_1 and in the magnetic field dependence of the profile. KBS, Kellar and Foster,[8] and Hernandez and Bryant[3] attempted to interpret the profiles quantitatively using classical Zeeman-limit theory (SBM Theory[10−12]) of NMR−PRE but concluded that this is not possible using physically realistic parameters. The reason for this unusual behavior has been studied by Bryant, Hodges, and Bryant (BHB),[6] who considered the possibility that the anomalously high relaxivity

* To whom correspondence should be addressed.

10.1021/jp046227o CCC: $30.25
Published on Web 03/23/2005

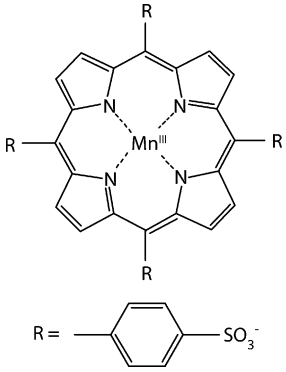

Figure 1. Manganese (III) meso-tetra(4-sulfonatophenyl)porphine chloride (Mn^{III}TSPP).

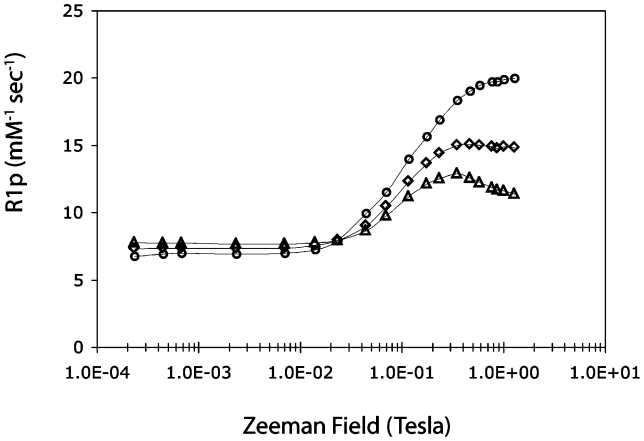

Figure 2. Proton R_1 magnetic relaxation dispersion profiles of aqueous Mn^{III}TSPP samples. The data, taken from ref 1, were measured at 5 °C (circles), 25 °C (diamonds), and 37 °C (triangles).

results from electron spin delocalization onto the porphyrin, but unrestricted Hartree−Fock calculations[13] have shown that the electron spin is highly localized on Mn(III).

BHB further suggested that zero-field splittings (zfs) of Mn(III) might underlie the unusual behavior. The quadratic cylindrical zfs parameter, $D = -3.16$ cm^{-1}, has been measured[14] for Mn^{III}TSPP by high-field ESR spectroscopy. This large value ensures that the electron spin system is in the vicinity of the zfs-limit over the experimental range of Zeeman field strengths ("zfs-limit" is the physical regime of magnetic field strengths where the zfs Hamiltonian is large compared to the electronic Zeeman Hamiltonian, $H_{zfs} \gg H_{Zeem}$). Using a form of NMR−PRE theory that incorporates zfs terms into the electron spin Hamiltonian, Abernathy et al.[15] simulated the experimental data, demonstrating that zfs interactions are indeed responsible for the unusual behavior. Quite surprisingly, the shape of the MRD profiles is determined principally by the 4th-order tetragonal component of the zfs tensor, B_4^4, rather than by D, even though D is much larger in magnitude than B_4^4. The effect of the B_4^4 term results physically from a relatively small splitting ($\Delta\epsilon \approx 0.33$ cm^{-1}) of the spin levels of the $m_S = \pm 2$ non-Kramers doublet. This splitting induces low-frequency coherent oscillations in the matrix elements of $\langle S_z \rangle$, which play a critical role in the relaxation mechanism.

To confirm these findings, we have collected new MRD data for polyacrylamide gel samples in which Mn^{III}TSPP is reorientationally immobilized. Suppression of Brownian reorientation of the solute provides conditions in which the electron spin Hamiltonian is time-independent and considerably simplifies the analysis. However, our attempts to simulate both solution and gel data sets simultaneously using a single set of physical parameters (other than the reorientational correlation time) was not successful. It became clear that other important aspects of the relaxation mechanism (in addition to the B_4^4-induced doublet splitting) were involved. First, electron spin relaxation times differ within the three distinct non-Kramers manifolds ($m_S = 0, \pm 1, \pm 2$), as is expected from the fact that the interdoublet spacing is rather large (9.5 cm^{-1}). To account for multiple relaxation times, the expressions of NMR−PRE theory have been re-cast in the molecular frame (MF).

Another interesting aspect of the relaxation mechanism involves the effects of Brownian reorientation on the B_4^4-induced doublet splitting, which is partially reorientationally collapsed in liquid, but not in gel, samples. The 4th-rank zfs component, B_4^4, is randomized by a reorientational correlation time, $\tau_R^{(4)}$, which is considerably shorter than the reorientational correlation times of 1st and 2nd rank tensors (in general, $\tau_R^{(l)} \propto [l(l+1)]^{-1}$ for an lth-rank tensor). The splitting of the $m_S = \pm 2$ non-Kramers doublet is the primary determinant of the shape of the R_1 MRD profile, and the partial collapse of this splitting affects the MRD data.

Mn^{III}TSPP is a particularly important model system for NMR−PRE, since the principal phenomena that govern the relaxation mechanism differ so markedly (especially the role of the B_4^4-induced splitting) from those of other spins. It is particularly helpful for understanding the relaxation mechanism of this complex that the zfs D-parameter has been measured by ESR and that the orthorhombic zfs parameter (E) vanishes in the 4-fold site symmetry of the metal ion. The orientation of the zfs tensor is known, and the reorientational correlation time has been measured from ^{13}C T_1's of the diamagnetic analogue complex, Zn^{II}TSPP. The only physical parameters that are not known (or, at least, tightly constrained) from other experiments are B_4^4 and the electron spin relaxation times. The success of the simulations reported below for both gel and solution data indicate that the principal aspects of the relaxation mechanism are now satisfactorily understood. A recent study[16] of Fe^{III}TSPP ($S = 5/2$) shows that the 4th-order tetragonal zfs interaction is the critical determinant of the form of the MRD profile for this complex as well, although the role of the 4th-order zfs term in the relaxation mechanism is rather different for integer and half-integer spins.

Theory

NMR−PRE depends fundamentally on the electron spin level structure, the electron spin eigenfunctions, and spatial quantization of the spin motion. We first describe these in the vicinity of the zfs-limit for $S = 2$. We then summarize the major features of the NMR relaxation mechanism for Mn^{III}TSPP and write the MF expressions that are needed to describe doublet-specific electron spin relaxation.

Spin Hamiltonian and Level Diagram. For $S = 2$, the spin Hamiltonian, including zfs and Zeeman terms but neglecting nuclear-electron hyperfine terms, can be written

$$H_S = H_{Zeeman} + H_{zfs}^{\circ} \tag{1a}$$

$$H_{Zeeman} = g_e \beta_e \vec{B}_0 \cdot \vec{S} \tag{1b}$$

$$H_{zfs}^{\circ} = B_2^0 \hat{O}_2^0 + B_2^2 \hat{O}_2^2 + B_4^0 \hat{O}_4^0 + B_4^2 \hat{O}_4^2 + B_4^4 \hat{O}_4^4 \tag{1c}$$

In eq 1b, g_e, β_e, and $\vec{B}_0$ are the electron g factor, the Bohr magneton, and the Zeeman field strength. In eq 1c, the operator equivalents $\hat{O}_k^q$ of rank k and degree q are functions of the spin

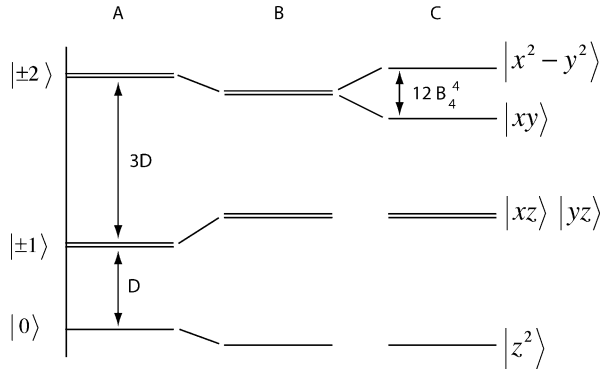

Figure 3. Spin energy levels and spin wave functions for $S = 2$ in the tetragonal zfs limit. Frames A−C show the effects of turning on successive components of the zfs tensor, (A) D only; (B) $D + B_4^0$; (C) $D + B_4^0 + B_4^4$.

operators, which are tabulated in Appendix A for $k = 2$ and 4. These functions vanish for $k > 2S$ due to the dimensionality of spin space, and they also vanish for odd k due to the reflection symmetry of the zfs tensor. The functions, $\hat{O}_k^q$, transform as $\cos(q\varphi)$ under rotations about the principal zfs axis, $\hat{z}$. For Mn^{III}-TSPP, the orthorhombic zfs terms ($q = 2$) vanish because of the 4-fold rotation symmetry, and H_{zfs}° is composed of two cylindrical ($q = 0$) and one tetragonal ($q = 4$) zfs terms

$$H_{zfs}^{\circ} = B_2^0\hat{O}_2^0 + B_4^0\hat{O}_4^0 + B_4^4\hat{O}_4^4 \qquad (1d)$$

Equations 1c and 1d are written in the molecule-fixed (MF) zfs principal axis system, denoted by a karat ($\wedge$). The coefficients B_k^q and $\tilde{B}_k^q$ have units of Joules and wavenumbers respectively, so that, $B_k^q = hc(10^2)\tilde{B}_k^q$, where Planck's constant h and the speed of light c are in SI. The quadratic zfs coefficients, $\tilde{B}_2^0$ and $\tilde{B}_2^2$ are related the zfs parameters D and E of ESR spectroscopy by $\tilde{B}_2^0 = D/3$ and $\tilde{B}_2^2 = E$.

Figure 3 shows the spin level diagram for $S = 2$ in the tetragonal zfs-limit. In this symmetry, the orthorhombic ($q = 2$) terms, B_2^2, B_4^2, vanish because of the 4-fold rotation axis of the crystal field (CF). This is the physical situation for the Mn^{III}-TSPP. In the cylindrical zfs-limit (Figure 3A), B_2^0 breaks the degeneracy of the five spin states into a singlet and two non-Kramers doublets ($m_S = 0, \pm1, \pm2$), split by D and $3D$. The B_4^0 term alters these splittings (Figure 3B), but it does not break the degeneracy of the non-Kramers doublets. Thus the cylindrical zfs terms, B_2^0 and B_4^0, determine the large interdoublet splittings. These splittings drive high frequency spin motions, which contribute insignificantly to the NMR−PRE. In terms of eq 3a in the following section, the off-diagonal spin matrix elements which couple levels split by B_2^0 and B_4^0 (i.e., the large interdoublet splittings) are associated with spectral density functions of negligible amplitude because the transition frequencies, $\omega_{\mu\nu}$, are large. The significance of the cylindrical zfs terms with respect to NMR−PRE is that they determine the spatial quantization of the electron spin motion, which is aligned in the MF rather than the LF. As long as the spin system remains in the vicinity of the zfs-limit, the magnitudes of B_2^0 and B_4^0 have very little influence on the shape of the MRD profile. In the cylindrical zfs-limit, the spin eigenfunctions are usually chosen as the circularly polarized eigenbasis of H_{zfs}°, i.e., $\{|0\rangle, |\pm1\rangle, |\pm2\rangle\}$ spatially quantized along $\hat{z}$. However, a Cartesian eigenbasis is an equally good choice.

The orthorhombic zfs terms (which are absent by symmetry in Mn(III)-TSPP), B_2^2 and B_4^2, couple levels with $\Delta m_S = \pm2$. These terms split the $m_S = \pm1$ doublet in first-order perturbation theory. The $m_S = \pm2$ doublet splits only in higher order. These small intradoublet splittings drive low-frequency spin motions, which are important for NMR−PRE because they are associated with spectral density functions of appreciable amplitude in eq 3a.

The tetragonal zfs term, B_4^4, arises from the 4-fold rotational component of the CF and is present in Mn(III)-TSPP. This term couples levels with $\Delta m_S = \pm4$ and thus splits the $m_S = \pm2$ non-Kramers doublet in first-order (Figure 3C). This term forces a Cartesian polarization on the spin eigenfunctions, which transform spatially like d orbitals:

$$|z^2\rangle = |0\rangle \qquad (2a)$$

$$|xz\rangle = 2^{-1/2}(-|+1\rangle + |-1\rangle) \qquad (2b)$$

$$|yz\rangle = 2^{-1/2}(|+1\rangle + |-1\rangle) \qquad (2c)$$

$$|x^2 - y^2\rangle = 2^{-1/2}(|+2\rangle + |-2\rangle) \qquad (2d)$$

$$|xy\rangle = 2^{-1/2}(|+2\rangle - |-2\rangle) \qquad (2e)$$

Outline of the Relaxation Mechanism for Mn^{III}TSPP. Because the interdoublet zfs splittings of Mn^{III}TSPP are rather large (3.16 and 9.48 cm^{-1}),[14] significant contributions to the NMR−PRE arise almost entirely from the intradoublet spin matrix elements, i.e., from spin matrix elements which couple eigenstates within specific non-Kramers doublets. Matrix elements which couple levels belonging to different non-Kramers doublets oscillate at high frequencies and produce very little dipolar power density in resonance with the motions of the nuclear magnetic moment.

In the cylindrical zfs limit, the only low-frequency nonvanishing spin matrix elements are those of $\langle\hat{S}_z\rangle$, which is diagonal and a constant of the motion. For $S = 2$, the contributions of the $|0\rangle$, $|\pm1\rangle$, and $|\pm2\rangle$ doublet manifolds to the NMR−PRE vary as $m_S^2 = 0{:}1{:}4$, assuming equal electron spin relaxation times. When the zfs tensor is cylindrical, approximately 80% of the NMR relaxation efficiency arises from the $m_S = \pm2$ doublet. As described above, the B_4^4 term forces a Cartesian polarization on the spin wave functions (eq 2), as a result of which $\langle\hat{S}_z\rangle$ is no longer diagonal within the Cartesian eigenbasis. The only nonvanishing matrix element of $\langle\hat{S}_z\rangle$ within the $m_S = \pm2$ manifold is off-diagonal, namely, $\langle xy|\hat{S}_z|x^2 - y^2\rangle$, which oscillates at the B_4^4-induced doublet splitting of $12\ B_4^4$. Thus, $\langle\hat{S}_z(t)\hat{S}_z(0)\rangle$, which was a constant of the motion in the cylindrical zfs limit, is forced into oscillation at the intradoublet splitting ($12\ B_4^4$), with the result that the NMR relaxation efficiency due to the $m_S = \pm2$ levels is largely suppressed. Equivalently, the spectral density functions in eq 3a that are associated with matrix elements of $\langle\hat{S}_z\rangle$ within the $m_S = \pm2$ non-Kramers doublet are strongly suppressed by the B_4^4-induced spin oscillation.

The principal dispersive feature in the MRD profile of Mn-(III)-TSPP (Figure 2) is the rise in $R_{1\rho}$ that occurs at field strengths, $B_0 \approx 0.03$ T. This rise results almost entirely from a Zeeman-induced change in spin wave functions within the $m_S = \pm2$ manifold. When $B_0 \approx 0$, the spin wave functions have a Cartesian polarization, and the contribution of the $m_S = \pm2$ levels to R_{1M} is very small because of the B_4^4-induced spin oscillation. When, with increasing B_0, the Zeeman energy exceeds the doublet splitting, the spin wave functions change from Cartesian to cylindrical polarization $\{|0\rangle, |\pm1\rangle, |\pm2\rangle\}$, thereby generating diagonal matrix elements in $\langle\hat{S}_z\rangle$ which are

responsible for the rise of R_{1M}. A quantitative description of these phenomena is the objective of the study.

Theoretical Description. Our analysis of experimental data used the program Parelax2, the current version of which has been described.[17] Parelax2 implements four levels of theory, namely, (1) spin dynamics (SD) simulation; (2,3) "constant H_S" formulations of theory cast in the laboratory frame (LF) and the molecular frame (MF); and (4) a zfs-limit formulation cast in the MF. Of these, SD describes the effects of Brownian reorientation realistically but the algorithms cannot incorporate multiexponential electron spin relaxation. The "constant H_S" formulations are capable of describing multiexponential electron spin relaxation, but they ignore the effects of Brownian reorientation of H°_{zfs} in eq 1a.

In the present study, the MF "constant H_S" formulation provides the most useful description. The spin system of Mn^{III}-TSPP lies in the vicinity of the zfs limit; hence, an MF formulation is appropriate. Also, multiexponential electron spin relaxation, which can be incorporated into the "constant H_S" formulations but not in SD, was found to be important for Mn^{III}-TSPP. Third, solute reorientation is virtually eliminated in the gel samples and is relatively slow in solution samples, again suggesting the use of "constant H_S". The MF "constant H_S" expression for R_{1M} is the following:

$$R_{1M} = -48\pi(\gamma_I g_e \beta_e)^2 r_{IS}^{-6}(\mu_0/4\pi)^2 \sum_{q,q'=-1}^{1}\sum_{p,p'=-1}^{1} \times \begin{Bmatrix} 1 & 2 & 1 \\ p & (q-p) & -q \end{Bmatrix}\begin{Bmatrix} 1 & 2 & 1 \\ p' & (-q'-p') & q' \end{Bmatrix} \times (-1)^{q+q'} Y_{2,q-p}(\hat{\theta},\hat{\varphi}) Y_{2,q'-p'}(\hat{\theta},\hat{\varphi}) \times \{\mathscr{D}^{(1)}_{q,+1}(\alpha,\beta,\gamma)\mathscr{D}^{(1)}_{q',-1}(\alpha,\beta,\gamma) \times (2S+1)^{-1}\sum_{\mu,\nu}\langle\mu|\hat{S}^{(1)}_p|\nu\rangle\langle\nu|\hat{S}^{(1)}_{p'}|\mu\rangle\, \hat{j}_p(\omega_{\mu\nu})\}_{ea} \quad (3a)$$

$$j_p(\omega_{\mu\nu}) = \frac{\hat{\tau}^{(\mu)}_{d,p}}{1+(\omega_I-\omega_{\mu\nu})^2(\hat{\tau}^{(\mu)}_{d,p})^2} \quad (3b)$$

The quantities in braces are 3-j symbols, r_{IS} is the interspin distance, and μ_0 is permeability of space. The 2nd-rank spherical harmonics, $Y_{2,q}(\hat{\theta},\hat{\varphi})$, have as arguments the polar angles of $\vec{\mathbf{B}}_0$ with respect to the principal zfs axis, $\hat{z}$. The Wigner rotation matrix, $\mathscr{D}^{(1)}_{q,\pm1-p}(\alpha, \beta, \gamma)$, rotates operators from the laboratory frame to the MF through the Euler angles, (α, β, γ), and ea indicates an ensemble average over molecular orientations. Superscripting karats ($\wedge$) on spin and space variables denote that they are defined in the MF with respect to the zfs principal axes. The spin matrixes, $\langle\hat{S}^{(1)}_p\rangle$, are evaluated in the eigenbasis, $\{|\mu\rangle, |\nu\rangle\}$, of H_S.

The dipolar correlation time, $\hat{\tau}^{(\mu)}_{d,p}$, in eq 3b is defined as follows:

$$(\hat{\tau}^{(\mu)}_{d,p})^{-1} = (\tau^{(1)}_R)^{-1} + (\hat{\tau}^{(\mu)}_{S,p})^{-1} + (\tau_M)^{-1} \quad (4)$$

where the subscript p labels the spatial polarization $(\hat{x},\hat{y},\hat{z})$ and μ is the spin eigenstate. This quantity differs from that of Zeeman-limit theory. First, the reorientational correlation time, $\tau^{(1)}_R$, describes the motion of a 1st-rank, rather than a 2nd-rank, molecule-fixed tensor, as is appropriate in the zfs limit,[18] when the electron spin motion is quantized in the MF rather than the LF. The quantities, $\hat{\tau}^{(\mu)}_{S,p}$, describe the thermal decay of the matrix elements of the electron spin TCF's

$$G_{p,p'}(\tau) = \{\langle\hat{S}^{(1)}_p(\tau)\hat{S}^{(1)}_{p'}(0)\rangle\}_{ea}, \quad (p, p' = 0, \pm1) \quad (5)$$

with respect to the MF, rather than the LF. Further information about the treatment of electron spin relaxation within Parelax2 is given in refs 17 and 19−21. τ_M is the chemical exchange residence time of solvent protons in the metal coordination sphere.

Experimental Section

Manganese(III) meso-tetra(4-sulfonatophenyl)porphine chloride (Mn^{III}TSPP) was purchased from Frontier Scientific (Logan, Utah). Aqueous buffered samples were prepared with Mn^{III}-TSPP concentrations between 1.0 and 1.2 mM porphyrin in a series of buffers at pH 1−12 with total buffer concentrations of 50.0 mM. Hydrion dry buffer salts from Aldrich were used for the aqueous buffered samples of pH 2−12 (buffer composition: pH 2, 3 were biphthalate/sulfamic acid, pH 4 was biphthalate, pH 5, 6, 7, 8, 11, and 12 were phosphate, and pH 9 and 10 were carbonate). The pH 1 buffer was the certified standard from Fisher Scientific. The samples were placed in 7 mm acid-washed borosilicate test tubes, degassed by a series of five freeze−pump−thaw cycles and sealed under vacuum.

A series of gelled Mn^{III}TSPP samples were prepared using either polyacrylamide (PA) or gelatin as the immobilizing matrix. The PA samples were buffered at pH 6.2 or 7.5 using MES, HEPES, or phosphate buffers, to a total buffer concentration of 20 mM. PA samples were prepared from acrylamide and *N*,*N*′-methylenebisacrylamide (both electrophoresis grade), with *N*,*N*′,*N*″,*N*‴-tetramethylethylenediamine (TMED) as the propagator and ammonium persulfate as the initiator. Reagents were used as received from Aldrich. PA gels were prepared under nitrogen atmosphere, using freshly boiled water and TMED that had been degassed by five freeze−pump−thaw cycles. All reagents except the initiator were combined to make a stock acrylamide solution containing 20.15% T, 5.05% C, and 0.10% (v/v) propagator. An aliquot of freshly prepared 0.10% w/v ammonium persulfate was added to initiate polymerization. A sample containing 1.09 mM Mn^{III}TSPP in 20.2% w/v gelatin was prepared by dissolving gelatin (J. T. Baker) in boiling water, adding solid Mn^{III}TSPP to the warm solution, then diluting with cool water to the final concentration.

All glassware and sample tubes were soaked in concentrated nitric or sulfuric acid overnight before use to leach contaminating metals. Distilled, deionized water was taken from a Barnsted Millipore Filtration System with both ionic and organic sections that used deionized water as the feed. UV−visible absorption spectra were collected on a Shimadzu UV1601 spectrometer. Viscosities for the pre-gelled polyacrylamide samples (20% acrylamide) were measured in an Ostwald viscometer. NMR T_1 relaxation times were measured[22] at frequencies 0.6−70 MHz at 20 °C using a custom built tunable NMR spectrometer.[23]

Results

Figure 4A shows MRD data for the following samples (20°C): (a) Mn^{III}TSPP immobilized in a polyacrylamide gel (squares), (b) Mn^{III}TSPP immobilized in gelatin (circles), (c) Mn^{III}TSPP in the polyacrylamide solution prior to initiation of the polymerization reaction (diamonds), and (d) Mn^{III}TSPP in an aqueous buffer at pH 8 (triangles). Comparison of the profile of the post-gelation PA sample with that of the pre-gelation PA solution shows that gelation has immobilized Mn^{III}TSPP as expected. The PA and gelatin samples show similar solute immobilization up to $B_0 = 1$ T, above which the profiles

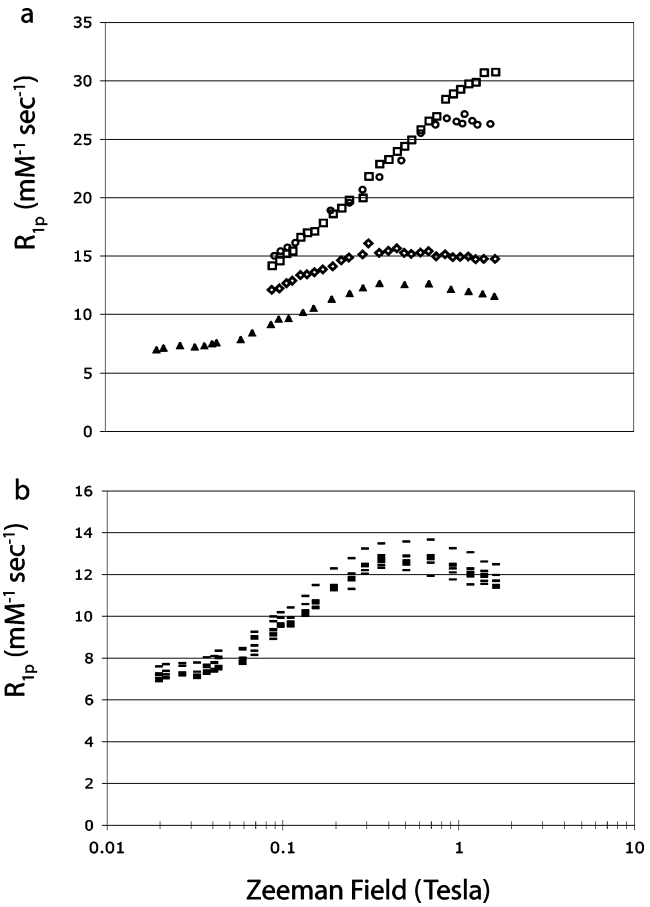

Figure 4. MRD profiles of the water proton R_{1p} of $Mn^{III}TSPP$ in various media at 20 °C. Frame A shows the effect of solute immobilization in a gel matrix. The samples (top to bottom) contained polyacrylamide gel (20% T + 5% C, pH 7.4, squares); gelatin (20% w/v, circles). Profiles are also shown for the acrylamide monomer solution prior to gelation (diamonds) and for a pH 8 aqueous buffered sample without the gel component (triangles). Frame B shows the effect of pH on the MRD profiles of samples prepared using pH 1−4 and 7−9 buffers (see text). The profiles are for samples with buffers, from top to bottom, of pH = 7, 4, 2, 9, 8, 3, and 1.

diverge. The difference in the MRD profiles of the pre-gelation PA sample and the buffered aqueous sample reflects the higher viscosity of the former.

pH Dependence. Figure 4B shows the MRD profiles for $Mn^{III}TSPP$ buffered at 10 integral values of pH from pH 1−12. The data were found to be nearly pH independent, in contrast to the previous report of Lyon, et al [2] in which R_{1p} at 10.7 MHz for $Mn^{III}TSPP$ decreased by 50% between pH 6 and 12. The reason for this difference is not known, although the sample compositions differed in that our samples contained 50 mM buffers, whereas the samples of Lyon et al were aqueous solutions with pH adjusted by addition of either HCl or NaOH.

Properties of the Gel Samples. Although $Mn^{III}TSPP$ is immobilized in the PA gel, the water solvent retains mobility similar to that of a simple aqueous solution. For dissolved species with dimensions ≥1 nm, translational and reorientational diffusion constants can be quite dependent on gel composition[24−8] thus affecting the background R_1. In control experiments, R_1 of the water solvent was found to be almost unaffected by the gel. Figure 5 shows changes in the water proton R_1 of a PA solution as a function of time during polymerization. Addition of the persulfate initiator (arrow) was followed by a transient R_1 decrease due temperature rise. After the temperature reequilibrated, R_1 was within 3% of that of the pre-gelation solution.

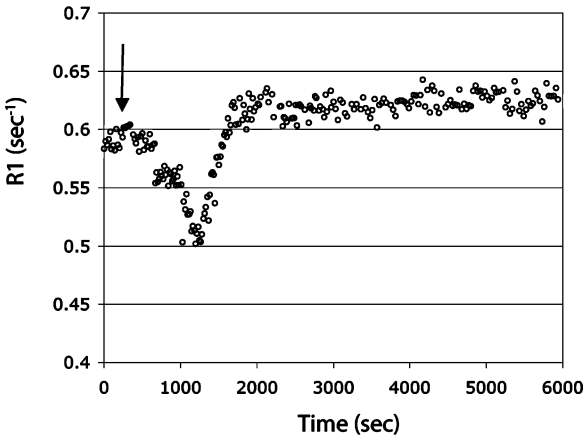

Figure 5. Time course of the diamagnetic background of the solvent proton R_1 during polymerization of a polyacrylamide sample (20% T + 5% C). Arrow indicates initiation of polymerization by addition of ammonium persulfate (0.1% w/v).

The porous structure of PA gels has been studied extensively, both experimentally and by theoretical modeling. For NMR studies, the PA concentration (20% T + 5% C) selected corresponds approximately to the minimum achievable pore diameter. At this concentration, the maximum pore diameter as measured by gel electrophoresis[29,30] is about 1.5 nm. As measured by NMR relaxation of water protons, the average pore diameter is <1.3 nm.[31] Higher concentrations of monomer and cross-linker lead to phase separation and sample inhomogeneity.[32,33] In comparison, the longest distance between sulfonate oxygens in $Mn^{III}TSPP$ is 2.2 nm. Thus, we expect $Mn^{III}TSPP$ to be tightly enmeshed in the gel lattice. This picture of a highly mobile solvent and a reorientationally immobilized solute has been confirmed by others in similar PAA gel systems using NMR measurements of water proton relaxation[34,35] and self-diffusion,[36,37] as well as by fluorescence.[38] However, librational motions of the solute are possible. The difference at high field strength between the MRD profiles measured in PA and gelatin gels probably reflects somewhat greater mobility of the gelatin matrix.

Control Experiments. In other control experiments, PA gel samples were monitored by UV−vis spectroscopy over the course of four months to examine chemical stability of Mn^{III}-TSPP as a function of time, particularly the possibility that manganese oxidation or reduction might result from free radicals generated during gelation. Spectra[39] prior to and following initiation of the polymerization reaction exhibited neither band shifts nor the appearance of new bands, characteristics indicative of changes in oxidation state.[40] It is well-known that solute aggregation occurs in aqueous H_2TSPP[41,42] and in solutions of some metalated TSPP solutes,[43,44] The possibility of aggregation in our samples was examined by UV−vis control experiments[45] and found to be absent.

Fits to the Theory. Five data sets were fit with the MF slow motion theory, shown in Figure 6. The samples used for this are $Mn^{III}TSPP$: (1) immobilized in polyacrylamide gel at 20 °C; (2) dissolved in the pre-gelation polyacrylamide solution at 20 °C; (3) dissolved in an aqueous buffered (pH 8) solution at 20 °C; (4) data from Bryant, Hodges, and Bryant[6] at 25 °C, and (5) data from Kellar and Foster[7] at 25 °C. The MRD profiles have been corrected for the outer sphere[46] and diamagnetic background contributions to R_{1p}, and are normalized to mM^{-1} for direct comparison.

Fixed Parameters. The NMR−PRE of $Mn^{III}TSPP$ depends on eight physical parameters, namely, (1)−(2) the quadratic zfs

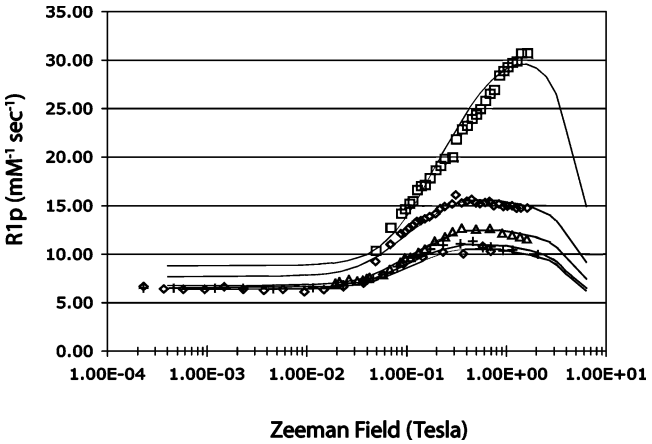

Figure 6. Theoretical simulations of Mn^{III}TSPP MRD profiles. The experimental data are taken from Figure 4 and from refs 6 (crosses) and 7 (diamonds). The samples contained, from top to bottom: gelled polyacrylamide (20 °C, squares), the acrylamide monomer solution prior to gelation (20 °C, diamonds), and a control sample lacking gel components (pH 8, 20 °C, triangles). The profiles taken from refs 6 (crosses) and 7 (diamonds) were measured at 25 °C.

parameters D and E, (3) the 4th-order zfs parameter, B_4^4, (4) the interspin distance r_{IS}, (5) the angle θ_{IS} between $\vec{r}_{IS}$ and $\hat{z}$, (6) the reorientational correlation time of a molecule-fixed first rank tensor, $\tau_R^{(1)}$, and the two eigenstate-specific electron spin relaxation times, (7) $\tau_S^{(\pm1)}$, and (8) $\tau_S^{(\pm2)}$ (the contribution of the $m_S = 0$ level to the NMR−PRE is negligible). The quadratic zfs parameters have been measured for Mn^{III}TSPP in a frozen aqueous solution by ESR[14] at 287 Ghz. The measured values are $D = -3.16(2)$ cm^{-1} and $E = 0$. The polar angle, $\theta_{IS} \approx 0.28$ rad, is representative of O−M−H angles for metal coordinated water derived from neutron diffraction studies on aqueous solutions of divalent metal ions.[47] From the crystal structure[48] of the related complex, $Mn^{III}TPP{\cdot}2H_2O$ (TPP = tetraphenylporphine), we assumed $r_{IS} = 0.282$ nm. The solution structure uncertainty in θ_{IS} and r_{IS} was estimated by allowing the tilt angle of the water ligand to vary from 0° to 90° with the metal oxygen distance fixed. This range of tilt produced variations of $\theta_{IS} = 0.28 \pm 0.06$ rad and $r_{IS} = 2.84 \pm 0.12$ Å. Variations of θ_{IS} within this range have very little effect on the calculations. The distance, r_{IS}, was permitted to vary between 2.72 and 2.96 Å.

The second rank reorientational correlation time, $\tau_{R,\hat{x}}^{(2)} = 275$ ps, has been measured[6] by ^{13}C T_1 relaxation of the pyrrole carbons of the diamagnetic analogue Zn^{II}TSPP in aqueous solution. $\tau_{R,\hat{x}}^{(2)}$ describes reorientation of a C−H dipolar tensor oriented in the porphyrin plane. The reorientational motion of Mn^{III}TSPP is significantly anisotropic, and the reorientational correlation time, $\tau_{R,\hat{z}}^{(2)}$, of the $\hat{z}$ axis (which is the approximate direction of $\vec{r}_{IS}$) is longer than $\tau_{R,\hat{x}}^{(2)}$. Appendix B describes the anisotropy correction, which gives $\tau_{R,\hat{z}}^{(2)} = 520$ ps. It should be noted that in the zfs limit the electron spin motion is quantized along molecule-fixed axes, and reorientation of the I−S dipolar interaction is described by the 1st-rank correlation time, $\tau_{R,\hat{z}}^{(1)} = 3\tau_{R,\hat{z}}^{(2)}$, rather than by $\tau_{R,\hat{z}}^{(2)}$.

Varied Parameters. The parameters varied in the simulations were $r_{IS} = 2.84 \pm 0.12$, $\Delta\epsilon_{\pm2}^{\circ} = 12B_4^4$ (the splitting of the $|\pm2\rangle$ manifold), $\tau_S^{(\pm1)}$ and $\tau_S^{(\pm2)}$. It will be shown below that $\tau_S^{(0)}$ does not contribute significantly within the field range of the experimental data.

Results of the Simulations. The results of the fits are shown in Figure 6 and Table 1. The fitting error for solution data was <1%, and for the gelled sample <6%. The values obtained for $\tau_S^{(\pm1)}$ and r_{IS}, the electron spin relaxation time of the $|\pm1\rangle$ manifold and the electron proton interspin distance, respectively, for the best fits are constant within experimental error. However, attempts to fit the data, even approximately, with a single electron spin relaxation time or with a single value of $\Delta\epsilon_{\pm2}^{\circ}$ were unsuccessful. Acceptable fits were obtained only when

1. $\Delta\epsilon_{\pm2,gel}^{\circ} > \Delta\epsilon_{\pm2,solution}^{\circ}$,
2. $\tau_S^{(\pm1)} \neq \tau_S^{(\pm2)}$,

and

3. $\tau_S^{(\pm2)}$ was allowed to vary by sample, lengthening substantially upon gelation.

TABLE 1: Summary of Fits[a]

	BHB[6]	FK[7]	buffer (aq)	pregelled	gelled
$\tau_{R,\theta=0}^{(2)}$ (ps)[a]	520	520	590	740	
$\tau_S^{(\pm1)}$ (ps)	460	470	480	480	500
$\tau_S^{(\pm2)}$ (ps)	115	120	145	170	390
$\Delta\epsilon_{\pm2}^{\circ}$ (cm^{-1})	.204	.192	.194	.170	.330
r_{IS} (Å)	2.83	2.84	2.83	2.80	2.82

[a] All fits used[14] $D = 3.16$ cm^{-1}, $E = 0.0$, $\theta_{IS} = 0.28$ rad. The calculations used a first rank dipolar correlation time, $\tau_R^{(1)} = 3\tau_R^{(2)}$, as is appropriate for the zfs limit. Different electron spin relaxation times, $\tau_S^{(\pm1)}$ and $\tau_S^{(\pm2)}$, were used for the $m_S = \pm1$ and $m_S = \pm2$ Kramers doublets. Tabulated values of $\tau_R^{(2)}$ were calculated as described in Appendix B and corrected for differences in temperature and viscosity, using the tabulated viscosity (η) of water and the measured viscosity of the 20% w/v pregelled solution. It was assumed that the gelled sample contained reorientationally immobilized solute. NMR−PRE data for the pregelled, gelled, and aqueous buffered samples from this laboratory were measured at $T = 293$ K, whereas data from refs 6 and 7 were run at $T = 298$ K.

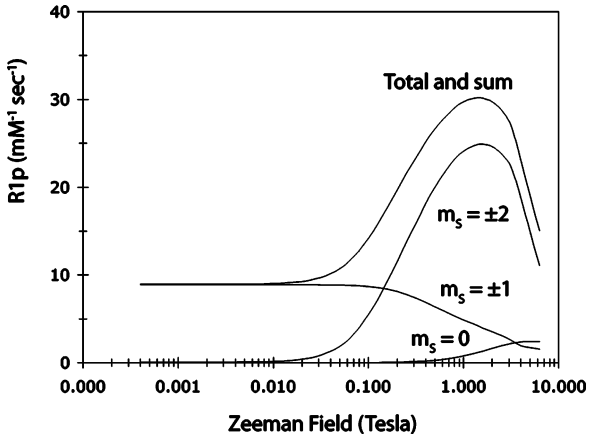

Figure 7. Contributions of the $m_S = 0$, ±1, and ±2 spin manifolds to the MRD profile of Mn^{III}TSPP in a polyacrylamide gel matrix.

***R*$_1$ Contributions of the Three Non-Kramers Doublets.** As described above, R_{1M} results almost entirely from contributions of the intradoublet spin matrix elements, i.e., matrix elements which couple levels belonging to the same non-Kramers doublet. The contributions of the $m_S = 0$, ±1, ±2 non-Kramers doublets to the MRD profile of the gel sample are shown in Figure 7. In the vicinity of the zfs limit, the $m_S = 0$ and ±2 levels contribute negligibly to R_{1M}, which is determined almost entirely by diagonal matrix elements within the $m_S = \pm1$ doublet manifold. When the Zeeman field reaches the vicinity of 0.03 T, the Zeeman energy is comparable to the B_4^4-induced splitting of the $m_S = \pm2$ manifold, and the $m_S = \pm2$ spin wave functions change, resulting in the generation of large diagonal matrix elements in $\langle\hat{S}_z\rangle$. These contribute strongly to the NMR−PRE

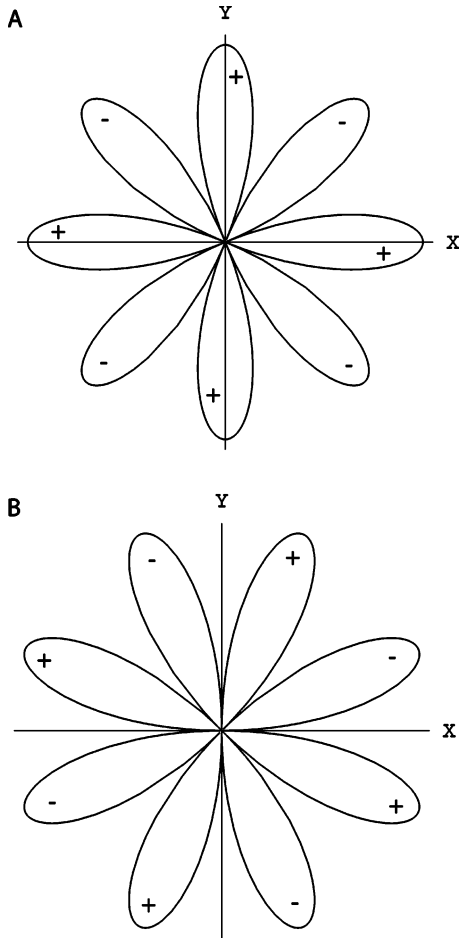

Figure 8. Variation of the tetragonal 4th-order spin operators on rotation about the 4-fold axis: (A) $\hat{S}_x^4 - \hat{S}_y^4$; (B) $(\hat{S}_x^2 - \hat{S}_y^2)\hat{S}_x\hat{S}_y$.

and are responsible for the rising dispersive feature. In Figure 7, the curve labeled "Total" includes all terms of eq 3. The curve labeled "Sum" shows the sum of intradoublet contributions of the three spin manifolds, neglecting the interdoublet terms. The results of these calculations were nearly identical, confirming that the contributions of the interdoublet spin matrix elements in eq 3 are negligible.

Discussion

Effects of Partial Motional Collapse of the $m_S = \pm 2$ Doublet Splitting. The observation that the $m_S = \pm 2$ doublet splitting is smaller in solution than in gelled samples appears to result from partial motional collapse of the doublet structure. The 4th-order splitting arises from the interaction of the spin wave functions with the 4-fold rotational component of the CF. When molecular rotation about the 4-fold axis is rapid, the CF potential is averaged, and the splitting collapses. The doublet splitting in the gel (where Brownian reorientation is inhibited) is 0.3 cm^{-1}, or 5.65×10^{10} rad s^{-1}. Collapse of the splitting occurs when the motional correlation time is the order of 20 ps.

The reorientational correlation time for tumbling of a second rank tensor oriented along the $\hat{z}$ axis of Mn^{III}TSPP, $\tau_{R,\hat{z}}^{(2)}$, is approximately 520 ps in solution. This is based on the measured value for the reorientational correlation time of BHB,[6] correction for anisotropic reorientation (see below and Appendix B). The correlation time of the fourth rank interaction, $B_4^4\hat{O}_4^4$, that is responsible for the $m_S = \pm 2$ splitting is much shorter than this. The physical situation is illustrated in Figure 8A, which shows the $\cos(4\varphi)$ spatial variation of the spin operator $\hat{O}_4^4$. Molecular rotation about $\hat{z}$ transforms $\hat{O}_4^4 \rightarrow -\hat{O}_4^4 \rightarrow \hat{O}_4^4$ as φ passes from $0 \rightarrow \pi/4 \rightarrow \pi/2$. Thus, rotation by $\pi/2$ rad about $\hat{z}$ inverts, and restores, the fourth order interaction. In general, the decay of the time correlation function of an *l*th-rank tensor due to rotation about $\hat{z}$ is described by a correlation time

$$\tau_{\hat{z}}^{(l)} = [l(l+1)D_{||}]^{-1} \tag{6}$$

where $D_{||}$ is the diffusion coefficient for rotation about $\hat{z}$.

This correlation time of eq 6 is quite different from $\tau_{R,\hat{z}}^{(l)}$ (eq B3a, Appendix B), which describes Brownian tumbling of the $\hat{z}$ axis itself, a process that depends on rotation about the axes perpendicular to $\hat{z}$, i.e., upon $D_\perp$. For a highly oblate spheroid like Mn^{III}TSPP, rotation about $\hat{z}$ is faster than rotation about $\hat{x}$ or $\hat{y}$, because the latter motions require displacement of more solvent than the former. Hu and Zwanzig[49] have calculated hydrodynamic friction coefficients for oblate and prolate spheroids as a function of principal axis ratio. Modeling Mn^{III}-TSPP as an oblate spheroid with axis ratio (3.5/21), Hu and Zwanzig's tabulations give the ratio, $D_{||}/D_\perp \approx 3.5$. This ratio, used in conjunction with Huntress' theory of anisotropic reorientation[50] and the measured correlation time, $\tau_{R,\hat{x}}^{(2)} = 275$ ps,[6] gives the value, $\tau_{R,\hat{z}}^{(2)} = 520$ ps, for reorientation of a 2nd−rank tensor oriented along $\hat{z}$.

The 4th-order correlation time for rotation about $\hat{z}$ is $\tau_{\hat{z}}^{(4)} = 44$ ps (Appendix B). Because $\tau_{R,\hat{z}}^{(4)} > \hbar/\Delta\epsilon_{\pm 2}^{\circ}$, the level structure does not coalesce, but the doublet spacing decreases and the $m_S = \pm 2$ levels are broadened. We consider this a probable explanation for why $\Delta\epsilon_{\pm 2,gel}^{\circ} > \Delta\epsilon_{\pm 2,solution}^{\circ}$.

Effects of the $m_S = \pm 2$ Doublet Splitting on Electron Spin Relaxation. The rapid motion described by $\tau_{R,\hat{z}}^{(4)}$ also acts to shorten $\tau_S^{(\pm 2)}$. Electron spin relaxation of the $m_S = \pm 2$ levels is produced primarily by intradoublet spin transitions because the interdoublet spacing between the $m_S = \pm 1$ and ± 2 levels is large, 9.5 cm^{-1}. Molecular reorientation about $\hat{z}$ induces stochastic terms in HS that couple the $m_S = \pm 2$ levels and induce intradoublet transitions. Rotation about $\hat{z}$ transforms the $\hat{O}_4^4$ spin function into the spin function

$$(\hat{O}_4^4)' = (\hat{S}_x^2 - \hat{S}_y^2)\hat{S}_x\hat{S}_y \tag{7}$$

The fourth order functions, $\hat{O}_4^4$ and $(\hat{O}_4^4)'$, are related by a $\pi/8$ rotation about $\hat{z}$ (see Figure 8B). The O_4^4 term of the static spin hamilton splits the $m_S = \pm 2$ non-Kramers doublet, whereas the stochastic term, $(\hat{B}_4^4)'(\hat{O}_4^4)'$, induces $\Delta m_S = \pm 4$ transitions between $m_S = \pm 2$ levels. This acts to shorten $\tau_S^{(\pm 2)}$ in the liquid samples, as observed.

Summary

The NMR−PRE due to the $S = 2$ complex Mn^{III}TSPP is produced by a unique physical mechanism in which the 4th-order tetragonal component, B_4^4, of the zfs tensor plays the principal role. In the zfs limit, the B_4^4 term splits the $m_S = \pm 2$ non-Kramers doublet and drives the matrix elements of $\langle \hat{S}_z \rangle$ into oscillation at the frequency of the doublet splitting. This oscillation acts to decouple resonant energy transfer between the nuclear and electron spins thus suppressing the NMR−PRE. The principal dispersive feature of the MRD profile is a profound rise in R_1 at the Zeeman field strengths where the 1Q Zeeman energy exceeds the B_4^4-induced doublet splitting. In this regime of field strengths, the electron spin wave functions

change character and diagonal matrix elements of $\langle \hat{S}_z \rangle$ become large. The NMR−PRE is especially sensitive to the diagonal spin matrix elements (which contribute low-frequency dipolar power), and thus, R_1 increases in magnitude in this regime. B_4^4 is the principal physical parameter on which the shape of the profile depends.

To test this mechanism, we have measured MRD profiles of samples in which Mn^{III}TSPP is reorientationally immobilized in a gel matrix. Four sets of gel and solution MRD data were analyzed simultaneously using a single set of physical parameters, all of which were known (or tightly constrained) from prior experiments except B_4^4 and two electron spin relaxation times, $\tau_S^{(\pm 1)}$ and $\tau_S^{(\pm 2)}$. Satisfactory fits to the data required (1) different electron spin relaxation times for the $m_S = \pm 1$ and ± 2 non-Kramers doublet manifolds; (2) a B_4^4 parameter that is smaller in solution than in the gel samples; (3) an electron spin relaxation time, $\tau_S^{(\pm 2)}$, that is shorter in solution than the gels. Findings (2) and (3) appear to result from a partial collapse of the B_4^4-induced doublet splitting due to Brownian reorientation.

After accounting for the effects of Brownian motion on the splitting of the $m_S = \pm 2$ levels and on $\tau_S^{(\pm 2)}$, the MRD data have been simulated quantitatively by theory. The principal aspects of the relaxation mechanism appear now to be satisfactorily understood.

Acknowledgment. This material is based upon work supported by the National Science Foundation under Grant No. CHE-0209616.

Supporting Information Available: A complete description of the NMR experimental technique is provided in the Supporting Information. Tests were performed to determine the stability of Mn^{III}TSPP in solution, with the results shown in Figure 1S-A. Tests for porphyrin aggregation were run, and the results are shown in Figure 1S-B. The estimated crystal structure of Mn^{III}TSPP is shown in Figure 2S, and a description for how it was determined is given. This was necessary to determine a distance of closest approach, shown in Figure 3S, that was necessary to calculate the outer sphere contribution to the NMR−PRE. Outer-sphere and scalar contributions to R_{1M} were estimated and found to be negligible. This material is available free of charge via the Internet at http://pubs.acs.org.

Appendix A

The spin functions, O_k^q, used in eq 1c are taken from Table 16 in Appendix B of Abragam and Bleaney.[51] $\{(A), (B)\}_S$ is the symmetrized operator, 2^{-1} $(AB + BA)$

$$O_2^0 = 3S_z^2 - S(S+1) \tag{A1}$$

$$O_2^2 = 2^{-1}(S_+^2 + S_-^2) = (S_x^2 - S_y^2) \tag{A2}$$

$$O_4^0 = 35S_z^4 - 30S(S+1)S_z^2 + 25S_z^2 - 6S(S+1) + 3S^2(S+1)^2 \tag{A3}$$

$$O_4^2 = 2^{-1}\{(7S_z^2 - S(S-1) - 5), (S_+^2 + S_-^2)\}_S \tag{A4}$$

$$O_4^4 = 2^{-1}(S_+^4 + S_-^4) \tag{A5}$$

Appendix B

Anisotropic Reorientational Correlation Time. The reorientational correlation time $\tau_R^{(2)}$ has been measured by ^{13}C T_1 relaxation for the pyrrole carbons of the aqueous diamagnetic analogue Mn^{III}TSPP. This value,[6] $\tau_R^{(2)} = 275$ ps at 298 K, describes reorientation of a C−H interspin (I−S) vector in the porphyrin plane. The NMR−PRE depends on the Mn−H vector, which lies close to the $\hat{z}$ axis. Because of anisotropic reorientation, the tumbling motion of $\hat{z}$ is slower than that of a vector in the molecular plane. Corrected values of the correlation times were calculated using Huntress' hydrodynamic model[50] of anisotropic reorientation and Hu and Zwanzig's tabulated values[49] of anisotropic frictional torque coefficients.

The rotational diffusion constant, D_i, for motion about the ith principal axis of the moment of inertia, is related to the frictional torque coefficient for that axis, ξ_i, by[50]

$$D_i = k_B T/\xi_i \tag{B1}$$

For a symmetric rotor, the lth-rank reorientational correlation times for motion of $\vec{r}_{IS}$, denoted $\tau_{R,IS}^{(l)}(\theta)$, is related to the rotational diffusion constants via:[50,52,53]

$$\tau_{R,IS}^{(l)}(\theta) = \frac{1}{l(l+1)D_\perp} \times \left\{1 + \frac{3(D_\perp - D_\parallel)\sin^2\theta}{5D_\perp + D_\parallel}\left[1 + \frac{3(D_\perp - D_\parallel)\sin^2\theta}{2(D_\perp + 2D_\parallel)}\right]\right\} \tag{B2}$$

where θ is the angle between $\hat{z}$ and $\vec{r}_{IS}$.

Setting $D_r = D_\perp/D_\parallel$, and noting that when $\theta = 0$, $\tau_{R,IS}^{(l)}(\theta) = \tau_{R,z}^{(l)}$ and when $\theta = \pi/2$, $\tau_{R,IS}^{(l)}(\theta) = \tau_{R,x}^{(l)}$, eq B2 gives

$$\tau_{R,z}^{(l)} = \frac{1}{l(l+1)D_\perp} \tag{B3a}$$

and

$$\tau_{R,x}^{(l)} = \frac{1}{l(l+1)D_\perp}\left\{1 + \frac{3(D_r - 1)}{5D_r + 1}\left[1 + \frac{3(D_r - 1)}{2(D_r + 2)}\right]\right\} \tag{B3b}$$

Combining eqs B3a and B3b, an expression for the ratio of the reorientational correlation times, $(\tau_{R,z}^{(l)}/\tau_{R,x}^{(l)})$, is obtained in terms of the ratio of diffusion coefficients, D_r.

The ratio of diffusion coefficients was estimated using eq B1 in conjunction with Hu and Zwanzig's hydrodynamic friction coefficients. Mn^{III}TSPP can be approximated as an oblate spheroid with principal axis lengths, 3.5 and 21 nm. From the ratio of the principal axes lengths, $\rho = 0.16$, Hu and Zwanzig's tabulated values[49] of frictional torque coefficients gives

$$\frac{\xi_\perp}{\xi_\parallel} = \frac{1}{D_r} \cong 3.5 \tag{B4}$$

From eqs B3a and B3b, $\tau_{R,z}^{(l)} \cong 1.89^*\tau_{R,x}^{(l)}$. Using the measured value, $\tau_{R,x}^{(2)} = 275$ ps, gives $\tau_{R,z}^{(2)} = 520$ ps for Mn^{III}TSPP at 298 K. The rotational diffusion constants are $D_\perp = 3.2 \times 10^8$ s^{-1} and $D_\parallel = 1.1 \times 10^9$ s^{-1}. From eq 6 of the text, $\tau_{\hat{z}}^{(4)} = 44$ ps for rotational motion about $\hat{z}$.

References and Notes

(1) Koenig, S. H.; Brown, R. D. III; Spillar, M. *Magn. Reson. Med.* **1987**, *4*, 252.
(2) Lyon, R. C.; Faustino, P. J.; Cohen, J. S.; Katz, A.; Mornex, F.; Colcher, D.; Baglin, C.; Koenig, S. H.; Hambright, P. *Magn. Reson. Med.* **1987**, *4*, 24.
(3) Hernandez, G.; Bryant, R. G. *Bioconjugate Chem.* **1991**, *2*, 394.
(4) Sur, S.; Bryant, R. G. *J. Phys. Chem.* **1995**, *99*, 4900.

(5) Bradshaw, J. E.; Gillogly, K. A.; Wilson, L. J.; Kumar, K.; Wan, X.; Tweedle, M. F.; Hernandez, G.; Bryant, R. G. *Inorg. Chim. Acta* **1998**, *275*−*276*, 106.
(6) Bryant, L. H.; Hodges, M. W.; Bryant, R. G. *Inorg. Chem.* **1999**, *38*, 1002.
(7) Kellar, K. E.; Foster, N. *Inorg. Chem.* **1992**, *31*, 1353.
(8) Kellar, K. E.; Foster, N. *Anal. Chem.* **1991**, *63*, 2919.
(9) Chen, C.-W.; Cohen, J. S.; Myers, C. E.; Sohn, M. *FEBS Lett.* **1984**, *168*, 70.
(10) Solomon, I. *Phys. Rev.* **1955**, *99*, 559.
(11) Bloembergen, N. *J. Chem. Phys.* **1957**, *27*, 572. **1957**, *27*, 595.
(12) Bloembergen, N.; Morgan, L. O. *J. Chem. Phys.* **1961**, *34*, 842.
(13) Sahoo, N.; Das, T. P. *Hyperfine Interact.* **1990**, *61*, 1197.
(14) Krzystek, J.; Telser, J. *J. Magn. Res.* **2003**, *162*, 454.
(15) Abernathy, S. M.; Miller, J. C.; Lohr, L. L.; Sharp, R. R. *J. Chem. Phys.* **1998**, *109*, 4035.
(16) Schaefle, N.; Sharp, R. *J. Chem. Phys.* **2005**, in press.
(17) Schaefle, N.; Sharp, R. R. *J. Magn. Reson.* **2005**, submitted.
(18) Sharp, R. R. *J. Chem. Phys.* **1993**, *98*, 912.
(19) Sharp, R.; Lohr, L. *J. Chem. Phys.* **2001**,*115*, 5005.
(20) R. Sharp, *J. Magn. Reson.* **2002**, *154*, 269.
(21) Schaefle, N.; Sharp, R. *J. Chem. Phys.* **2004**, *121*, 5387.
(22) See Supporting Information for a description of the experimental technique.
(23) Bovet, J.-M.; Ph.D. Thesis, University of Michigan, Ann Arbor, MI, 1993.
(24) Gibbs, S. J.; Johnson, C. S. J., Jr.; *Macromolecules* **1991**, *24*, 6110.
(25) Pavesi, L.; Rigamonti, A. *Phys. Rev.* **1995**, *E51*, 3318.
(26) Pavesi, L.; Balzarini, M. *Magn. Reson. Imaging* **1996**, *14*, 985.
(27) Biermann, U. M.; Mikosch, W.; Dorfmuller, T.; Eimer, W. *J. Phys. Chem.* **1996**, *100*, 1705.
(28) Penke, B. Kinsey, S.; Gibbs. S. J.; Moerland, T. S.; Locke, B. R.; *J. Magn. Reson.* **1998**, *132*, 240.
(29) Holmes, D. L.; Stellwagen, N. C.; *Electrophoresis* **1991**, *12*, 253.
(30) Stellwagen, N. C.; *Electrophoresis* **1998**, *19*, 1542.
(31) Chui, M. M.; Phillips, R. J.; McCarthy, M. J.; *J. Colloid Interface Sci*. **1995**, *174*, 336.
(32) Derium A.; Cavatorta, F.; Asnaghi, D.; Bossi, A.; Righetti, P. G. *Physica B: Condens. Matter* **1997**, *234*−*236*, 271.
(33) Asnaghi, D.; Giglio, M. *Nuovo Cimento Soc. Ital. Fis., D* **1998**, *20D* (12bis), 2175.
(34) Penke, B.; Kinsey, S.; Gibbs, S. J.; Moerland, T. S.; Locke, B. R. *J. Magn. Reson*. **1998**, *132*, *240*.
(35) Pavesi, L.; Rigamoni, A. *Phys. Rev*. **1995**, *E51*, 3318.
(36) Haggerty, L.; Sugarman, J. H.; Prud'homme, R. K. *Polymer* **1988**, *29*, *1058*.
(37) Gibbs, S. J.; Johnson, C. S. *Macromolecules* **1991**, *24*, 6110.
(38) Biermann, U. M.; Mikosch, W.; Dorfmuller, T.; Eimer, W. *J. Phys. Chem.* **1996**, *100*, 1705.
(39) See Supporting Information for these spectra and detailed experimental description.
(40) Cotton, F. A.; Wilkinson, G.; Murillo, C. A.; Bochman, M.; *Advanced Inorganic Chemistry*, 6th ed.; Wiley-Interscience: New York, 1999.
(41) Akins, D. L.; Zhu, H.-R.; Guo, C. *J. Phys. Chem.* **1994**, *98*, 3612.
(42) Maiti, N. C.; Mazumdar, S.; Periasamy, N. *J. Phys. Chem. B* **1998**, *102*, 1528.
(43) Krishnamurthy, M.; Sutter, J. R.; Hambright, P. *J. Chem. Soc., Chem. Commun.* **1975**, 13.
(44) Hambright, P. In *The Porphyrin Handbook*; Kadish, K. M., Smith, K. M., Guilard, R., Eds.; Academic Press: New York, 2000; Vol. 3, Chapter 18.
(45) See Supporting Information for these spectra and detailed experimental description of these control experiments.
(46) The outer sphere R_1 contribution was estimated using combined SD/MD simulation techniques. These calculations are described in the supporting material.
(47) Powell, D. H.; Neilson, G. W.; Enderby, J. E. *J. Phys.: Condens. Matter* **1989**, *1*, 8721.
(48) Williamson, M. W.; Hill, C. L. *Inorg. Chem*. **1987**, *26*, 4155.
(49) Hu, C.-M.; Zwanzig, R. *J. Chem. Phys.* **1974**, *60*, 4354.
(50) Huntress, W. T. *Adv. Magn. Res*. **1970**, *4*, 1.
(51) Abragam, A.; Bleaney, B.; *Electron Paramagnetic Resonance of Transition Ions*, Oxford University Press: London, 1970; Chapter 16 and Appendices.
(52) Abragam, A. *The Principles of Nuclear Magnetism*; Oxford University Press: London, 1961; Chapter 8.
(53) Shimuzu, H. *J Chem. Phys.* **1964**, *40*, 754.